NASA/TM-2008-215529

Assessment of the LC-2 Prelaunch Fatigue Spectra of the CM-to-SM Flange Weld

David S. Dawicke
Analytical Services and Materials, Inc., Hampton, Virginia

John A. Newman
Langley Research Center, Hampton, Virginia

October 2008

The NASA STI Program Office . . . in Profile

Since its founding, NASA has been dedicated to the advancement of aeronautics and space science. The NASA Scientific and Technical Information (STI) Program Office plays a key part in helping NASA maintain this important role.

The NASA STI Program Office is operated by Langley Research Center, the lead center for NASA's scientific and technical information. The NASA STI Program Office provides access to the NASA STI Database, the largest collection of aeronautical and space science STI in the world. The Program Office is also NASA's institutional mechanism for disseminating the results of its research and development activities. These results are published by NASA in the NASA STI Report Series, which includes the following report types:

- TECHNICAL PUBLICATION. Reports of completed research or a major significant phase of research that present the results of NASA programs and include extensive data or theoretical analysis. Includes compilations of significant scientific and technical data and information deemed to be of continuing reference value. NASA counterpart of peer-reviewed formal professional papers, but having less stringent limitations on manuscript length and extent of graphic presentations.

- TECHNICAL MEMORANDUM. Scientific and technical findings that are preliminary or of specialized interest, e.g., quick release reports, working papers, and bibliographies that contain minimal annotation. Does not contain extensive analysis.

- CONTRACTOR REPORT. Scientific and technical findings by NASA-sponsored contractors and grantees.

- CONFERENCE PUBLICATION. Collected papers from scientific and technical conferences, symposia, seminars, or other meetings sponsored or co-sponsored by NASA.

- SPECIAL PUBLICATION. Scientific, technical, or historical information from NASA programs, projects, and missions, often concerned with subjects having substantial public interest.

- TECHNICAL TRANSLATION. English-language translations of foreign scientific and technical material pertinent to NASA's mission.

Specialized services that complement the STI Program Office's diverse offerings include creating custom thesauri, building customized databases, organizing and publishing research results ... even providing videos.

For more information about the NASA STI Program Office, see the following:

- Access the NASA STI Program Home Page at ***http://www.sti.nasa.gov***

- E-mail your question via the Internet to help@sti.nasa.gov

- Fax your question to the NASA STI Help Desk at (301) 621-0134

- Phone the NASA STI Help Desk at (301) 621-0390

- Write to:
  NASA STI Help Desk
  NASA Center for AeroSpace Information
  7115 Standard Drive
  Hanover, MD 21076-1320

NASA/TM-2008-215529

Assessment of the LC-2 Prelaunch Fatigue Spectra of the CM-to-SM Flange Weld

David S. Dawicke
Analytical Services and Materials, Inc., Hampton, Virginia

John A. Newman
Langley Research Center, Hampton, Virginia

National Aeronautics and
Space Administration

Langley Research Center
Hampton, Virginia 23681-2199

October 2008

Available from:

NASA Center for AeroSpace Information (CASI)
7115 Standard Drive
Hanover, MD 21076-1320
(301) 621-0390

National Technical Information Service (NTIS)
5285 Port Royal Road
Springfield, VA 22161-2171
(703) 605-6000

Abstract

The pad stay and rollout components of the Ares I-X life cycle can generate cyclic stress oscillations to the vehicle that could initiate and grow fatigue cracks from weld defects. The Ares I-X Project requested that a study be performed to determine if stabilization of the vehicle is required to reduce the stresses that could initiate and grow fatigue cracks at the flange-to-skin weld of the Command Module (CM) and Service Module (SM) interface.

A fatigue crack growth analysis was conducted that used loads (LC-2) and stress analyses developed by the Ares I-X Project and utilized material data and analysis methods developed by a critical initial flaw size (CIFS) analysis conducted by NASA Engineering and Safety Center (NESC) for the Upper Stage Simulator (USS) of the Ares I-X vehicle. A full CIFS analysis for the CM-to-SM flange-to-skin weld was not performed because the full flight spectrum was not provided and was not necessary to answer the question posed by the Ares I-X Project. Instead, an approach was developed to determine if the crack growth due to the pad stay and rollout components of the flight spectrum would adversely influence the CIFS. The approach taken used a number of conservative assumptions that eliminated the need for high-fidelity analyses and additional material testing, but still provided a bounding solution for the uncertainties of the problem.

The results from this analysis indicate that the LC-2 pad stay and rollout spectrum components would not produce significant fatigue crack growth on the CM-to-SM flange-to-skin weld. Thus, from a fatigue crack growth standpoint, no stabilization is required to reduce the LC-2 pad stay and rollout cyclic stresses on the CM-to-SM flange-to-skin weld.

Introduction

The Ares I-X vehicle consists of segments that are stacked together to form the complete vehicle, as illustrated in Figure 1. NASA Glenn Research Center (GRC) is responsible for the Interstage Module, the Upper Stage Simulator (USS) segments, and the Service Module (SM). NASA Langley Research Center (LaRC) is responsible for the Command Module (CM) and Launch Abort System (LAS). The individual segments are built separately and assembled at NASA Kennedy Space Center (KSC). The USS segments are manufactured using rolled sheets of 0.5 inch thick A516 Grade 70 steel for the skin and 1 inch thick A516 Grade 70 steel for the flange. Gussets are welded to the skin and flange every 10 degrees around the inside circumference. The two mating surfaces of the stacked segments are held together with bolts every 2 degrees. A critical initial flaw size (CIFS) assessment of the USS flange-to-skin welds has been performed by the NASA Engineering and Safety Center (NESC) [1]. The mating surfaces of the CM-to-SM interface contain a flange-to-skin weld that uses the same A516 Grade 70 steel as the USS structure. The configuration of the weld is similar to the USS weld, but no comparison of the two weld processes (heat inputs and post-weld normalization) was available at the time of this analysis. This analysis uses the material properties (crack growth rate and fracture toughness) determined from the NESC CIFS assessment of the USS welds, the rollout and pad stay spectrum components for the CM-to-SM interface,

and the local CM weld stresses to evaluate the influence of the spectrum components on crack growth damage.

The result of this analysis will be an assessment of whether stabilization is needed to reduce the stresses due to the rollout and pad stay spectrum components from a fatigue crack growth rate point-of-view. The approach will be to use conservative assumptions to simplify the required analyses. Only if necessary will the conservative assumptions be relaxed and supported with high-fidelity analyses and/or additional testing.

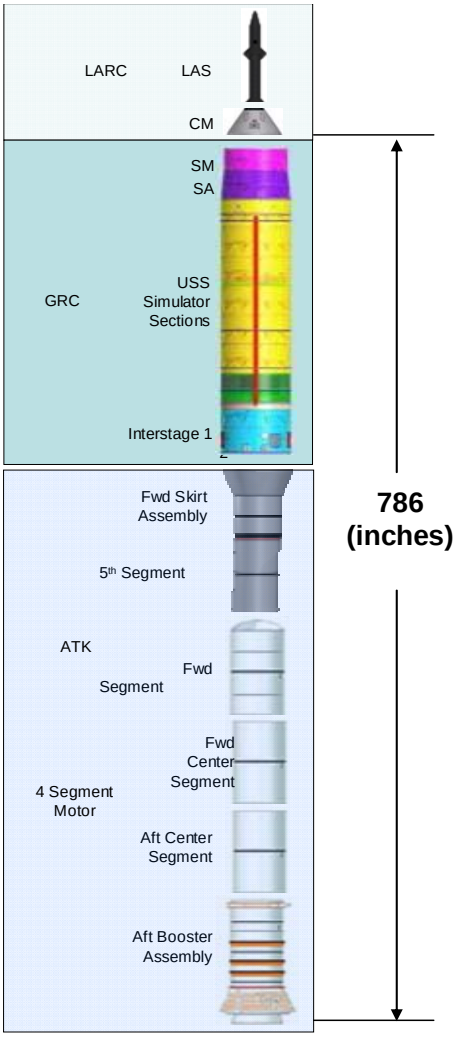

Figure 1. A schematic of the segments that make up the Ares I-X Vehicle.

Problem Description

An assessment is required to determine if the rollout and pad stay components of the Ares I-X LC-2 load spectrum will generate sufficient fatigue crack growth damage to the flange-to-skin weld at the CM-to-SM interface to require stabilization of the vehicle to reduce the magnitude and number of stress cycles. A full CIFS analysis will not be performed because the entire LC-2 load spectrum has not been made available for this analysis. Instead of a full CIFS analysis, an assessment of the maximum possible

contribution to the CIFS for the LC-2 rollout and pad stay spectrum components will be performed. This type of analysis can provide two possible recommendations:

- The crack growth that results from the LC-2 rollout and pad stay spectrum components are so small that they will have little or no influence on the CIFS regardless of the remaining LC-2 spectrum components. Hence, the conclusion can be made that no stabilization is necessary.
- The crack growth that results from the LC-2 rollout and pad stay spectrum are not small, so no conclusions regarding the need for stabilization can be made without a full CIFS analysis.

Critical Initial Flaw Size (CIFS) Concept

A CIFS analysis assumes an initial crack size (a_i) and grows that crack according to the material behavior (fatigue crack growth rate (da/dN) and fracture toughness (K_c)), loading spectrum for the structure, and the stress-intensity factor (K) for the crack configuration. The critical flaw size (a_{CFS}) is obtained when the maximum stress-intensity factor for any one cycle of the loading spectrum exceeds the fracture toughness value. The critical number of spectrum repeats necessary to grow the crack from a_i to a_{CFS} is N_c. The CIFS crack length (a_{CIFS}) is defined as the largest crack length that will survive four repeats of the spectrum ($N_c - 4$), as illustrated in Figure 2. A CIFS analysis requires the following information:

- Loading spectrum that accounts for the local stresses in the vicinity of the crack
- Stress-intensity factor solution (relationship between load and K)
- Material behavior that describes the fatigue crack growth rate (da/dN verses ΔK data)
- Material behavior that describes the critical stress-intensity factor (fracture toughness data)
- A fatigue crack growth rate code

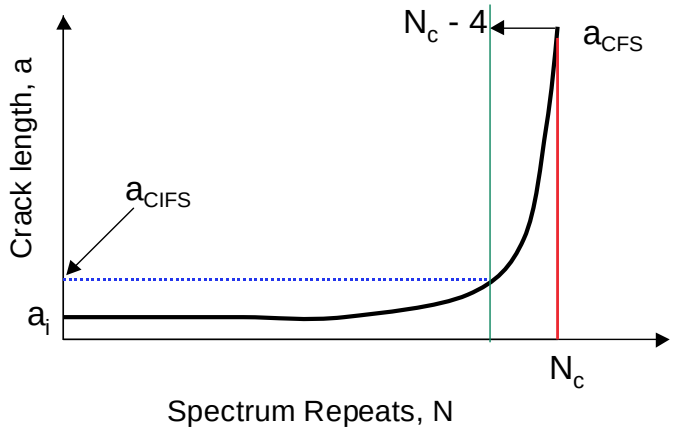

Figure 2. Schematic of the CIFS approach.

NESC Ares I-X USS Flange-to-Skin Weld CIFS Assessment

The NESC performed an independent assessment of the CIFS analysis of the flange-to-skin weld for the Ares I-X USS [1]. The assessment considered the influence of both surface cracks and embedded cracks that are shown schematically in Figure 3. The surface crack was found to be the limiting (conservative) crack configuration. The NESC assessment determined the CIFS for surface cracks with different aspect ratios (ratio of crack depth to surface crack length, a/2c), as illustrated in Figure 4. The CIFS results asymptotically approach a constant value for long shallow surface cracks as the length (2c)

approaches the width (or circumference) of the flange (W), and the stress-intensity factor solution approaches that of an edge crack. Likewise, the CIFS results approach those of a through-the-thickness crack as the crack depth approaches the thickness of the skin (t). Any crack that falls below the curve will not grow to a critical size in less than four repeats of the flight spectrum. The location and shape of the curve is dependent on the loading spectrum, crack geometry, material properties, etc.

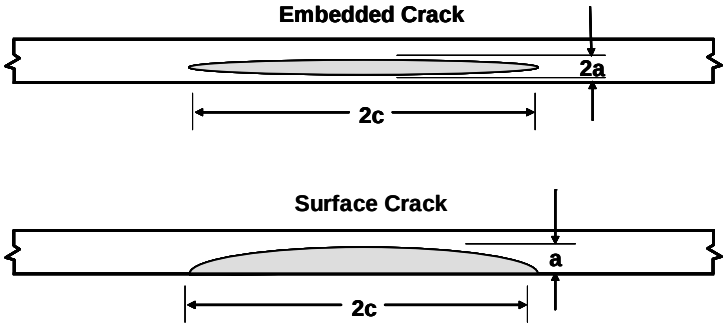

Figure 3. Schematic of the embedded and surface cracks.

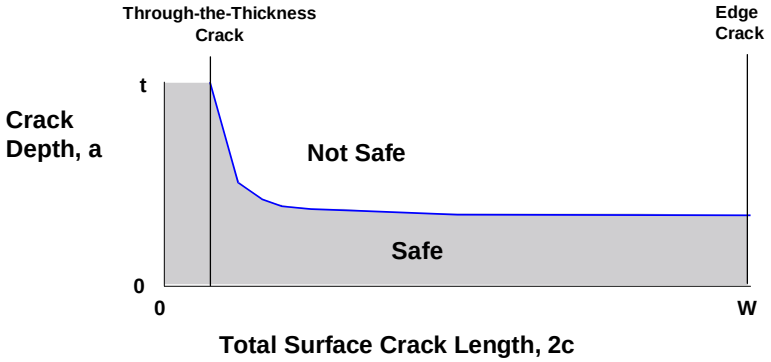

Figure 4. Schematic of the CIFS results.

The NESC CIFS analysis used a number of assumptions to allow the CIFS to be determined without extensive use of high-fidelity analyses and tests. The resulting CIFS was larger than the inspection size and did not present an additional burden to the manufacturing process, so the use of, less conservative, high-fidelity analyses that would result in larger CIFS values would not add value to the Ares I-X Project. The key assumptions from the NESC CIFS analysis (and used in the current analysis) are discussed below:

- **The fatigue crack threshold behavior was ignored**. A linear elastic fracture mechanics (LEFM) approach to predicting fatigue crack growth behavior assumes that the crack growth is related to the stress-intensity factor range (ΔK), independent of crack configuration. This means that the material behavior obtained from simple laboratory coupons can be used to predict the crack growth behavior in a more complex structure. The fatigue crack threshold is the stress intensity factor range (ΔK_{th}) below which no crack growth is observed. The A516 steel experiences a high mean stress fatigue crack threshold at a value around 3 ksi inch^{½}. The determination of a fatigue crack threshold would require extensive testing and the demonstration that the threshold obtained from laboratory coupons is appropriate for surface cracks in a weld. A conservative assumption would be to ignore that threshold and assume that any small stress cycles will cause fatigue damage.
- **The fracture toughness for a surface crack in the weld region will be greater than the elastic component of the J_{IC} value obtained from a J-R test conducted on a simple laboratory coupon.** The

A516 steel is a very ductile material and as a result of the extensive plasticity at the crack tip, the LEFM K_{IC} fracture toughness cannot be determined from the size of laboratory coupons that are available for the flange-to-skin weld. A fracture test that calculates the elastic plastic fracture mechanics (EPFM) parameter J as a function of crack growth can account for the plasticity in a ductile material [2]. However, to use this parameter in a CIFS analysis it must be shown that the value of J at the onset of crack growth (J_{IC}) determined for the laboratory coupon is appropriate for a surface crack in a weld. Rather than conduct extensive tests to demonstrate the similitude between laboratory coupons and surface cracks at welds, the NESC made an assumption that was considered to be very conservative. The parameter J consists of an elastic component and a plastic component that can be calculated from the experimental data. As ductility increases, the magnitude of the plastic component becomes larger and dominates the elastic component. For the Ares I-X USS assessment, the NESC used a fracture toughness obtained from only the smaller elastic component of the measured J_{IC} value.

- **The weld residual and fit-up stresses are tensile and constant through-the-thickness at a value equal to the material flow stress (average between the yield and ultimate stress).** The weld process can generate large tensile and compressive residual stresses. A mismatch of the mating flange surfaces can also generate residual stresses due to the forced closing of gaps during the application of the torque to the bolts. These residual stresses influence the CIFS by elevating the mean stress of the flight spectrum cycles. The weld residual stress distribution will be roughly equilibrated through-the-thickness and will be relieved due to repeated cycling and fatigue crack growth. The fit-up stresses generally have a bending characteristic with a peak tensile stress on one surface and a compressive (or at least lower tensile stress) on the opposite surface. The assumption of a mean stress equal to the material flow stress is intended as a worst-case upper bound, encompassing both the weld residual and the fit-up stresses.
- **Only the mode-I stresses cause fatigue crack growth damage.** The axial cyclic stresses will generate mode-I loading for circumferential cracks in the weld. The influence of mode-II and mode-III loading on fatigue crack growth rate is typically small compared to the mode-I component. A typical weld process for a flange-to-skin type weld will deposit material in a circumferential manner with multiple weld passes required on both the inside and outside surfaces. Defects can be generated when the weld material in one pass does not fuse to the previous pass (lack of fusion defects) or due to the contamination of the surface of a pass with a foreign material (slag inclusion defect). Both types of defects become potential initiation sites for circumferential cracks that experience mode-I loading under axial stresses.
- **The peak axial tensile and peak axial compressive cyclic stresses occur at the same location.** The body forces and moments on the structure can generate a complex stress distribution where the peak axial tensile and peak axial compressive stresses occur at different locations. A bounding condition would assume that both peaks occur at the same location. A relaxation of this assumption would require multiple CIFS analyses that consider the influence of cyclic stresses around the entire circumference of the structure.
- **The peak axial tensile and peak axial compressive cyclic stresses are constant around the circumference of the structure and do not change as the crack grows.** This is a worst case upper bound on the cyclic stresses because in the actual structure, a growing crack will experience a reduced stress field as the tip moves away from the peak location. A relaxation of this assumption would require that the full 3-D axial stress field be considered in the crack growth analysis.
- **The curvature of the shell will not have a significant influence on the stress-intensity factor of the circumferential cracks**. Handbook stress-intensity factors for circumferential cracks in thin shells have been generated for a limited range of crack configurations. Solutions for a greater range of crack configurations have been generated for flat plates. A comparison of the shell and flat plate stress-intensity factor solutions for through-the-thickness cracks in a 0.5 inch thick shell with a large radius of curvature (radius/thickness > 100) is shown in Figure 5. The stress-intensity factor for the crack in the shell is higher than that of the flat plat, and for cracks that have a length less than 10 times the shell thickness there is less than a 10% difference. Note that the comparison does not show the influence for surface cracks.
- **The cyclic load interaction effects are ignored, and high stress ratio (R) crack growth rate behavior is used**. This assumption ignores the beneficial effects of fatigue crack retardation due to tensile overloads and the detrimental effects of compressive underloads (that are minimized by a high mean stress).

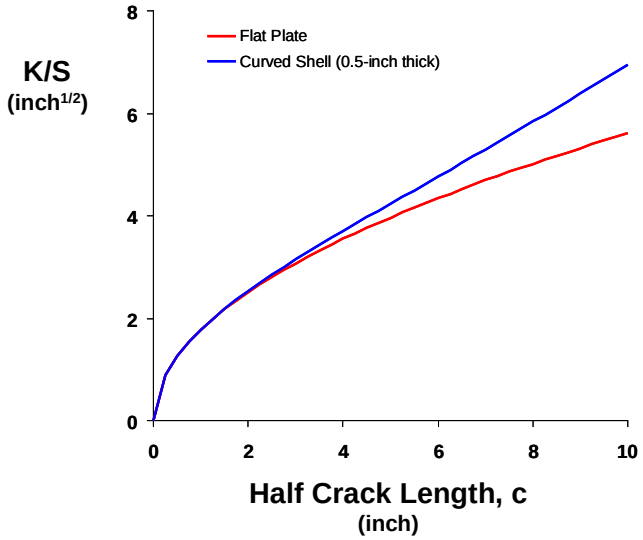

Figure 5. Comparison of the stress normalized stress-intensity factor (K/S) for a flat plate and curved shell.

Data Sources

The sources for the data used in the current LC-2 fatigue analysis of the CM-to-SM flange weld are provided in the following sub-sections.

F_x, M_y, and M_z Body Loads for Station 786

The F_x, M_y, and M_z body loads were provided for Station 786 [3] (the CM-to-SM interface at 786 inches from the vehicle base, as shown in Figure 1). The loads data consisted of the three body loads and the corresponding number of cycles (exceedences). A sample of the data file is shown in Table 1. The F_x load is provided in units of lbs., and the M_y and M_z moments are provided in units of lb-in. The body loads were determined for the eight flight components, or missions, as given in Table 2.

Table 1. Example of the body loads provided for Station 786.

FX	K14	MY	K54	MZ	K64
RANGE	NEXCEED	RANGE	NEXCEED	RANGE	NEXCEED
0.00E+00	27060475	0.00E+00	848445	0.00E+00	565440
2.00E+01	491532	5.00E+03	846644	5.00E+03	565222
4.00E+01	491332	1.00E+04	846644	1.00E+04	565218
6.00E+01	491312	1.50E+04	827836	1.50E+04	546328
8.00E+01	491301	2.00E+04	827836	2.00E+04	531231
1.00E+02	491283	2.50E+04	827833	2.50E+04	531227
1.20E+02	490670	3.00E+04	782114	3.00E+04	482006
1.40E+02	488644	3.50E+04	782113	3.50E+04	463184
1.60E+02	486310	4.00E+04	705834	4.00E+04	445817
1.80E+02	483302	4.50E+04	649012	4.50E+04	414488
2.00E+02	480685	5.00E+04	559145	5.00E+04	406938
2.20E+02	477952	5.50E+04	559088	5.50E+04	406932
2.40E+02	475981	6.00E+04	558525	6.00E+04	406920
2.60E+02	473846	6.50E+04	527673	6.50E+04	406306
2.80E+02	472166	7.00E+04	527634	7.00E+04	405562
3.00E+02	470506	7.50E+04	498549	7.50E+04	400917

Table 2. The definition of the eight flight spectrum components.

Event	Label
Rollout	Mission 001
30 day Pad Stay	Mission 002
Rollback	Mission 003
Rollout	Mission 004
20 day Pad Stay	Mission 005
Rollback	Mission 006
Rollout	Mission 007
10 day Pad Stay	Mission 008

Station 786 Time Consistent Axial Stresses

The body loads for Station 786 were not time consistent, with each of the three body loads having a different set of cycles, as shown in Table 1. Three different time-consistent spectra can be created by keying on each of the three body loads. For example, the K14 spectrum can be created by using the cycles associated with the F_x loads and using corresponding M_y and M_z moments. Three spectrum files K14, K54, and K64 were created that keyed on the F_x, M_y, and M_z body loads [4], respectively.

The body load components were used to calculate the axial stresses at the Station 786 weld location for the associated number of cycles. An example of the spectrum steps (pairs of max and min stress and the number of repeats) are shown in Table 3. The eight missions each contained more than 25,000 spectrum steps with many of the steps having little difference in the stress amplitude and mean stress. The eight missions were simplified by combining similar spectrum steps. The conservative approach of rounding up the maximum stress to the nearest 100 psi and rounding down the minimum stress to the nearest 100 psi was taken, as shown by the modified stresses in Table 3. The resulting simplification of the spectrum example is shown in Table 4. The three simplified spectrum files (K14, K54, and K64) are provided in Appendix A.

Table 3. A small example of the flight spectrum obtained from the body loads.

	Original Stresses		Modified Stresses	
Cycles	S_{max} (psi)	S_{min} (psi)	S_{max} (psi)	S_{min} (psi)
1	-55.2	-92.3	0	-100
589	-37.3	-92.3	0	-100
43	-43.8	-123.7	0	-200
48	119.3	-231.9	200	-300
8	132.8	-217.3	200	-300
1	145.6	-297.5	200	-300
32	213.9	-280.4	300	-300
29	-33.5	-97.8	0	-100
40	-7.1	-108.1	0	-200
1	-58.4	-117.2	0	-200
75	13.5	-89.2	100	-100
14	-27.3	-85.7	0	-100
10	-14.2	-119.9	0	-200
891	**Total Cycles**			

A graphical representation of the three spectra (K14, K54, and K64) is provided in Figure 6. The three spectra include the cycles from all 8 missions. The K54 and K64 spectra are very similar for all stress ranges. The only significant difference between the K14 spectrum and the other two is the large number of cycles (20 million) for the smallest stress range.

Table 4. The simplification of the flight spectrum example from Figure 8.

Cycles	S_{max} (psi)	S_{min} (psi)
633	0	-100
94	0	-200
57	200	-300
32	300	-300
75	100	-100
891	**Total Cycles**	

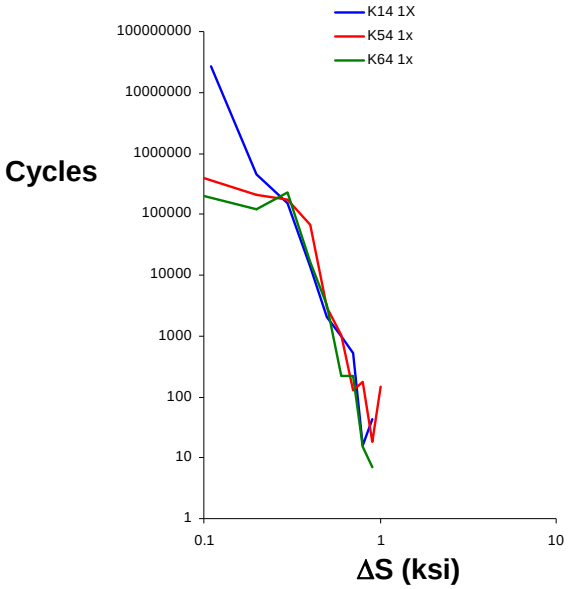

Figure 6. Graphical representation of the loading spectra used in the CM-to-SM flange-to-skin weld analysis.

Fatigue Crack Growth Rate Behavior

The NESC conducted fatigue crack growth rate tests to support the Ares I-X CIFS analyses [1]. The tests were conducted on ½ inch thick A516 steel plates obtained from the same lot of material that was used to construct the USS segments. The fatigue crack growth rate behavior of the weld material was not tested because the weld processes typically do not cause significant changes in the growth rate behavior of the steel. Two types of tests were conducted: constant R (the ratio of minimum stress to maximum stress, S_{min}/S_{max}) and threshold tests that were conducted at a constant maximum stress intensity factor (K_{max}) and an increasing stress ratio (R) [5]. The constant R tests were conducted for stress ratios of R = 0.3 and R = 0.7, and the results are shown in Figure 7. The threshold test was designed to yield a final stress ratio of R = 0.7 at a stress intensity factor range of ΔK = 2 ksi inch$^{1/2}$, as shown in Figure 7.

The test data were used to determine the coefficients to the NASGRO equation [6] given by Equation 1. The exponential parameters *p* and *q* were set to 0 to ignore threshold and K_{max} effects, resulting in a the simple power law relationship given by Equation 2. The empirical constants *c* and *n* were determined from the test data to be $6x10^{-10}$ and 2.8, respectively. Values of ΔK_{th} = 0.001 and K_c = 62 ksi inch$^{1/2}$ were used, but did not influence the crack growth rates calculated by Equation 1 because the *p* and *q* were set to 0. The curve fit to the experimental data is shown in Figure 7. Although the NASGRO equation curve fit parameters ignored threshold effects, a high stress ratio fatigue crack growth rate threshold of around 3 ksi inch$^{1/2}$ was measured for this material [1].

$$\frac{da}{dN} = \frac{c\Delta K^{n}\left(1-\frac{\Delta K_{th}}{\Delta K}\right)^{p}}{\left(1-\frac{K_{\max}}{K_{c}}\right)^{q}} \tag{1}$$

$$\frac{da}{dN} = c\Delta K^{n} \tag{2}$$

where, a = crack length,
N = number of cycles,
da/dN = crack growth rate,
c, n, p, and q = empirical constants,
ΔK = stress intensity factor range ($K_{max} - K_{min}$),
K_{max} = maximum cyclic stress intensity factor,
K_{min} = minimum cyclic stress intensity factor,
ΔK_{th} = threshold stress intensity factor range,
K_c = critical stress intensity factor

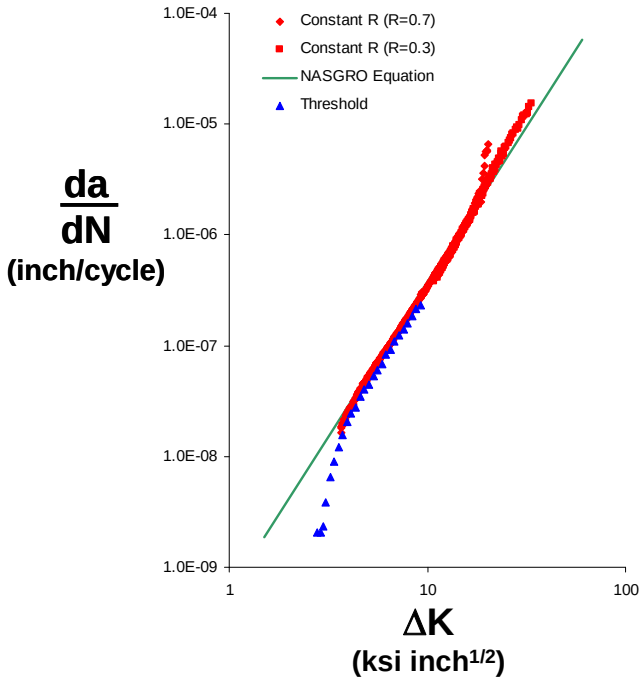

Figure 7. Fatigue crack growth rate test results and the NASGRO curve fit.

Fracture Toughness

The NESC conducted fracture tests on welded A516 steel in support of the Ares I-X CIFS assessment [1]. The material used in the testing was provided by the Ares I-X Project and was from the same lot as used to manufacture the USS segments. The weld process for the test was similar to, but not identical to, the final weld process for the flight structure. The fracture toughness was obtained from J_{IC} fracture tests conducted on 3-inch-wide compact tension (CT) specimens with the cracks located in the weld or the

heat-affected zone (HAZ). The testing was performed according to ASTM Standard 1820 [7] and met all requirements of the standard except those regarding the crack front shape. The weld and the resulting residual stresses were likely responsible for the irregular crack front shapes observed.

Three tests were conducted for each crack location, and the elastic component of J_{IC}, the plastic component of J_{IC}, and the total J_{IC} values were obtained from the measured load and crack mouth opening displacements. A 0.1/90% lower bound was determined from the test results. A concern about the similitude between a through-the-thickness crack in the test specimen and the surface crack in the actual structure resulted in a further reduction of the fracture toughness by considering only the elastic component of the measured J_{IC} value. A 0.1/90% lower bound of the three tests resulted in a fracture toughness, in terms of an LEFM stress-intensity factor, of $K_c = 62$ ksi inch$^{1/2}$.

Assumptions

The current fatigue crack growth analysis of the CM-to-SM flange-to-skin weld uses the same assumptions as used in the NESC Ares I-X USS CIFS analysis [1]. The following sub-sections provide additional details on the relevance of the assumptions for the CM-to-SM flange-to-skin weld.

Weld Fracture Toughness

The weld process for the CM-to-SM flange-to-skin weld is assumed to be similar, but not identical to, the weld used in the specimens tested during the NESC Ares I-X CIFS assessment. The use of the resulting fracture toughness of $K_c = 62$ ksi inch$^{1/2}$ was justified based on the conservativeness of the 0.1/90% lower bound and the use of only the elastic component of the measured J_{IC} value.

Weld Residual Stress

The NESC Ares I-X CIFS assessment conducted elastic-plastic finite element analyses to simulate the development of weld residual stresses [1]. These analyses incorporated the heat inputs from the weld process into a model that included local geometric details of the weld to determine the distortions and residual stresses. The analysis considered several different weld sequences that were considered for the welding of the USS segments. The results predicted a strong through-the-thickness variation in the weld residual stress that was bounded by a maximum value residual stress equal to the flow stress (57 ksi) of the material, as shown in Figure 8. As a conservative assumption, the weld residual stresses are assumed to be constant through-the-thickness and around the circumference of the flange and do not change as the crack grows (i.e., no stress redistribution). The weld residual stresses do not change the cyclic stress that dictate the crack growth rate, but instead act as a mean stress that elevates both the maximum and minimum stress. The elevation of the maximum stress dictates the critical crack length (stress-intensity factor equals the fracture toughness). The use of a mean stress equal to the flow stress was also assumed to accommodates the unknown fit-up stresses generated by the mating of mismatched flanges.

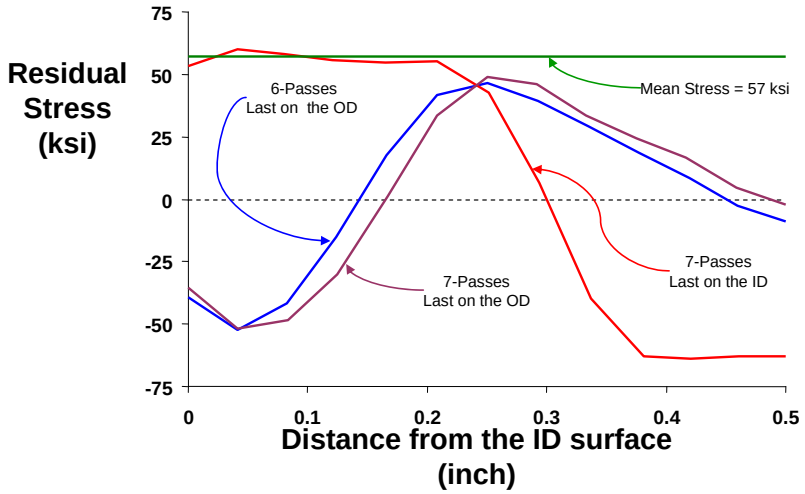

Figure 8. Weld residual stresses predicted for the NESC Ares I-X CIFS analysis.

Analysis Approach

The approach taken to determine the fatigue crack growth behavior of the CM-to-SM flange-to-skin weld was not to calculate a CIFS, but to determine the influence of the rollout and pad stay components of the spectrum. The NESC Ares I-X CIFS analysis [1] indicated that the surface crack was the limiting (most severe) configuration and hence only a surface crack configuration was considered in this analysis. The first step in the analysis was to determine the deepest or "best" possible critical crack depth (a_c) for surface cracks of different aspect ratios subjected to only the mean stress. This is the "best" possible critical crack length because any tensile axial stresses, when added to the mean stress, will result in smaller critical crack depths.

The second step in the analysis was to determine the rate that the crack is growing, due to the pad stay and rollout spectra components, as the crack approaches the critical depth (a_c). The amount of crack growth for the last four repeats of the spectrum is calculated (utilizing the CIFS requirement that the crack must survive four repeats of the spectrum), as illustrated in Figure 9. A slow growing crack will indicate that the spectrum component will not have a significant influence on the CIFS, regardless of the behavior of the rest of the flight spectrum. The top curve represents the "best" possible critical crack depth for surface cracks of different aspect ratios, and the middle and lowest curves represent schematically the expected influence of a slow and a fast rate of crack growth, respectively. This analysis can establish that stabilization would not be needed to reduce the stresses due to the rollout and pad stay spectrum components if the crack growth rate is slow. A complete CIFS analysis would be required if this analysis indicates that the crack growth rate for the two spectrum components is fast.

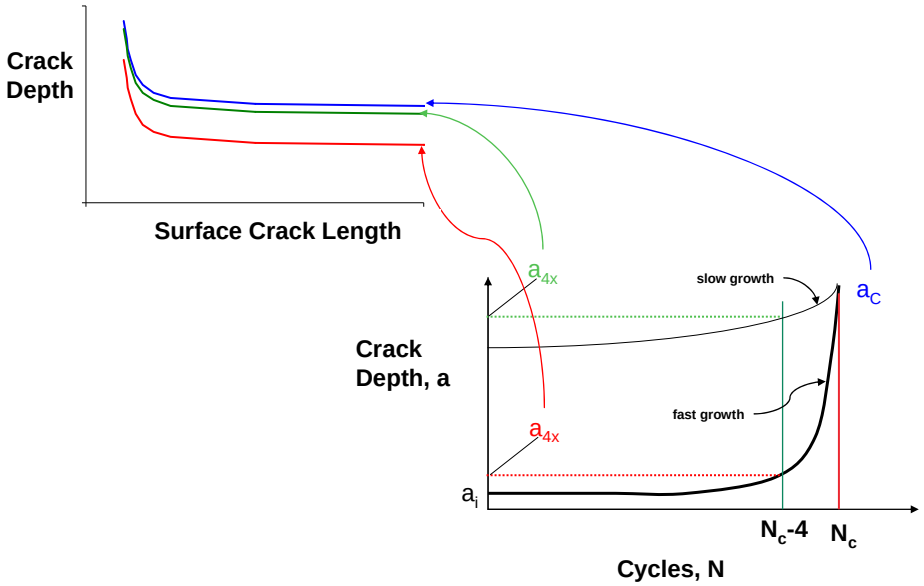

Figure 9. Schematic of the analysis approach.

Results

The fatigue crack growth behavior for the CM-to-SM flange-to-skin weld was calculated for the three spectra (K14, K54, and K64), as described in the previous sections. The aspect ratio of the crack (crack depth/crack length) was varied from 100 (long shallow cracks) to about 1 (semi-circular cracks).

a_c and a_{4x} Crack Growth

The "best" possible critical crack depth (a_c) was determined by calculating the crack size that results in a peak stress intensity factor equal to the fracture toughness of K_c = 62 ksi inch$^{1/2}$, as shown by the top curve of Figure 10. The largest crack sizes that will survive four repeats of the spectrum (a_{4x}) are also shown in Figure 10 for the three loading spectra. The K14 spectrum is the most severe, but the calculated a_{4x} values are only about 10% smaller than the corresponding a_c values for the same aspect ratio. The K54 and K64 spectra have calculated a_{4x} values that are only about 2% less than the corresponding a_c values.

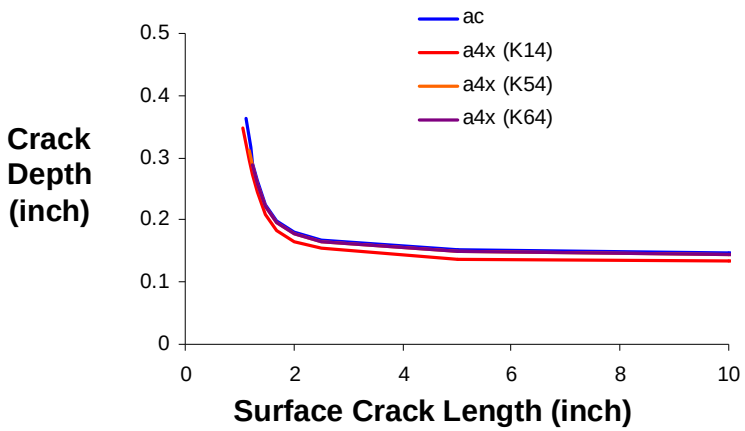

Figure 10. Calculated values of a_c and a_{4x} for the three spectra.

The K14 spectrum was scaled by factors of 3 and 10 ($K14_{3x}$ and $K14_{10x}$, respectively) to investigate the sensitivity of the crack growth behavior to uncertainties in the magnitude of the local stresses. The scaling was performed prior to the spectrum simplification of rounding up the stresses to the nearest 0.1 ksi. The scaling resulted in a translation of the curves to higher ΔS values as well as an increase in the number of spectrum steps, particularly at the higher ΔS values. The peak stress range increased from about 1 ksi for the original K14 spectrum to 10 ksi for the 10x scaling, as shown in Figure 11. Other than increasing the stress range, the most pronounced visual effect of the scaling was to spread out the very large number of cycles (more than 20,000,000) that were concentrated at the stress range of ΔS = 0.1 ksi in the original K14 spectrum. The $K14_{3x}$ spectrum resulted in calculated values of a_{4x} that were only slightly smaller than the original K14 spectrum, as shown in Figure 12. The $K14_{10x}$ spectrum resulted in calculated values of a_{4x} that were about 20% below the a_c values (0.116 inches and 0.144 inches, respectively).

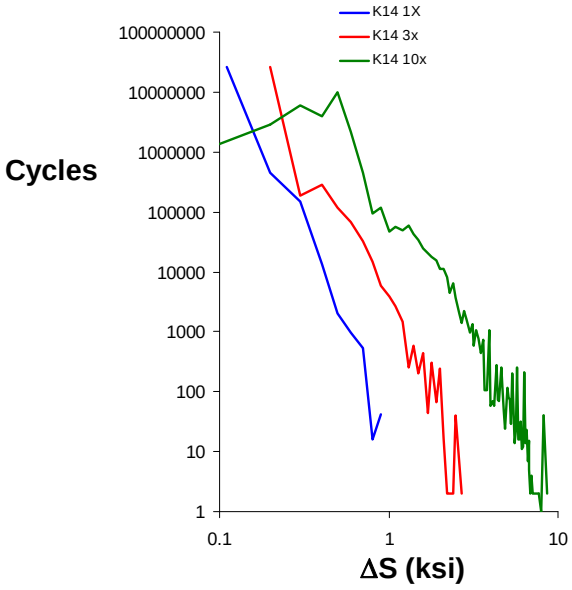

Figure 11. Visualization of the K14 load spectrum with a 1x, 3x, and 10x scale factor.

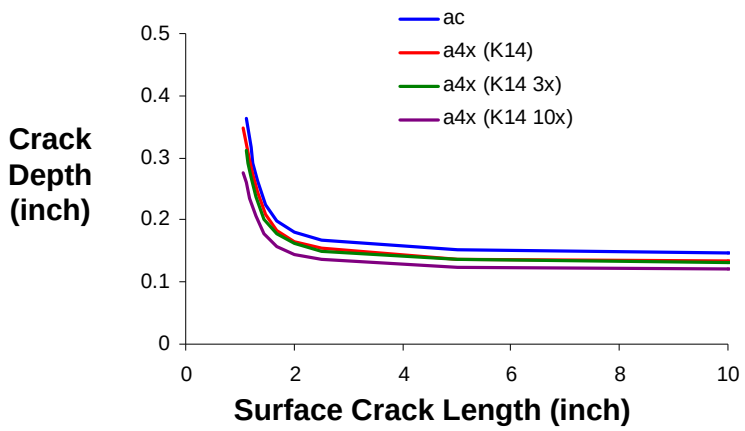

Figure 12. Calculated values of a_c and a_{4x} for the K14, $K14_{3x}$, and $K14_{10x}$ spectra.

Crack Growth of the K14 Spectra Components

The contributions of the individual loading steps of the K14, $K14_{3x}$, and $K14_{10x}$ spectra were determined by adding up the amount of crack growth for each stress range and comparing the value to the total crack growth, as shown in Figure 13. More than 98% of the crack growth damage from the original K14 spectrum was due to the large number of cycles (>20,000,000) at lowest stress range (ΔS = 0.1 ksi). About 95% of the crack growth damage from the $K14_{3x}$ spectrum was for stress ranges of 0.3 ksi and below. As with the original K14 spectrum, these stress ranges were associated with a large number of applied cycles. Only in the $K14_{10x}$ spectrum was the crack growth damage spread over a large number of loading steps. In this spectrum, about 95% of the crack growth damage was accounted for in stress ranges of 2.8 ksi and below.

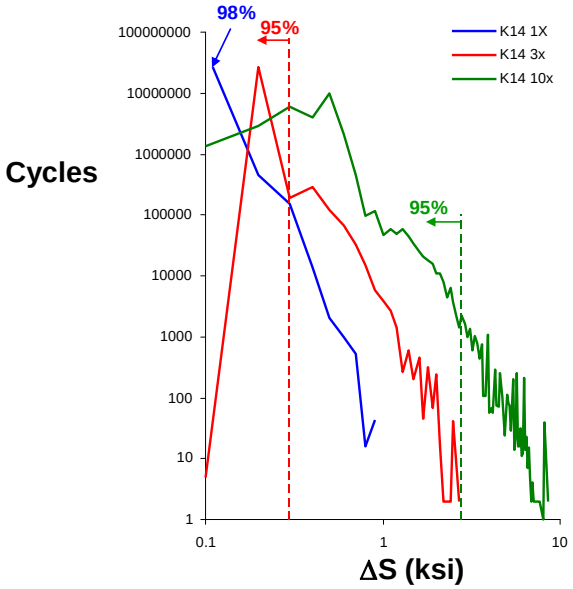

Figure 13. The contributions of crack growth damage for the K14, $K14_{3x}$, and $K14_{10x}$ spectra.

Fatigue Crack Threshold Comparison

The crack growth analysis used to evaluate the influence of the loading spectra assumed that the material did not experience a threshold (see Equ. 2). However, if a fatigue crack threshold (ΔK_{th}) did exist, then the influence of the spectrum steps that had a small stress range and a large number of cycles could be greatly diminished. This would result in slower crack growth rates, thus a smaller difference between the a_{4x} and the a_c crack depths. Note that the "best" possible crack depth (a_c) only considers the mean stress. The peak tensile cyclic stress, when added to the mean stress, would decrease the critical crack depth. The influence of a fatigue crack threshold on the ratio of the a_{4x} to a_c crack depths was calculated for different threshold values for the K14, $K14_{3x}$, and $K14_{10x}$ spectra, as shown in Figure 14. Very small threshold values (ΔK_{th} < 1 ksi inch$^{1/2}$) minimized the influence of the spectrum steps with small stress ranges and large cycles in both the K14 and $K14_{3x}$ spectra. For these two spectra, the ratio of a_{4x}/a_c was nearly 1, indicating that the remaining spectrum steps resulted in very slow fatigue crack growth rates. The ratios could never equal 1 because of non-zero tensile axial stresses, when added to the mean stress, would always produce a critical crack depth that was less than the a_c value. The predicted fatigue crack growth behavior for $K14_{10x}$ spectra was also influenced by threshold values less than about 1.5 ksi inch$^{1/2}$. However, the small number of cycles at the higher stresses will prohibit the ratio of a_{4x}/a_c from exceeding 0.95.

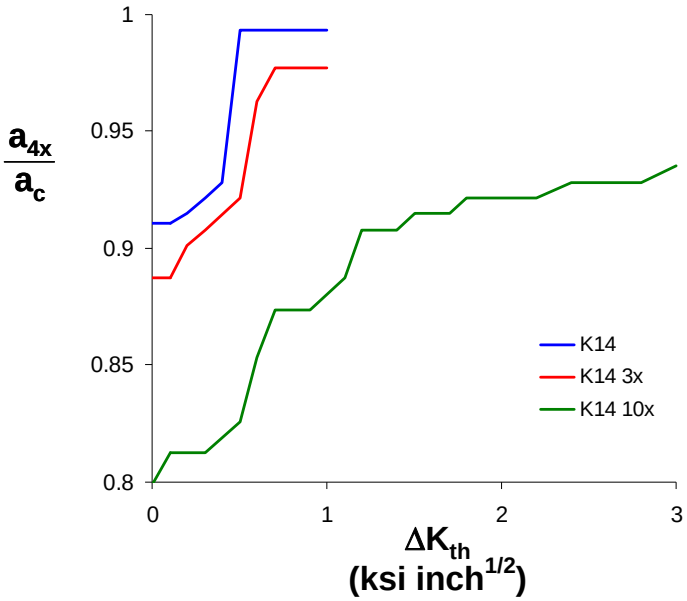

Figure 14. Influence of fatigue crack threshold (ΔKth) on the calculated fatigue crack growth rate behavior of the K14, $K14_{3x}$, and $K14_{10x}$ spectra.

Findings

The findings from the fatigue crack growth analysis of the CM-to-SM flange-to-skin weld are summarized below:

- The predicted fatigue crack growth for the K54 and K64 spectra indicated less than a 2% difference between a_{4x} and a_c values. This indicates that the crack growth rates due to these two spectra are negligible because the tensile axial stresses are too small and have too few cycles to significantly reduce the critical crack depth.

- The predicted fatigue crack growth for the K14 spectrum indicated about a 10% difference between the a_{4x} and a_c values. About 98% of the fatigue crack growth damage was due to the spectrum step with the lowest stress range and the highest number of cycles. Although the analysis ignored a fatigue crack growth threshold, the stress-intensity factor range that results from the lowest stress range spectrum step would, at less than 1 ksi inch$^{1/2}$, likely be below a conservative estimate of the threshold.
- The predicted fatigue crack growth for the $K14_{3x}$ spectrum was only slightly more damaging than the K14 spectrum. As with the K14 spectrum, the spectrum steps with the lowest stress range and the highest number of cycles were responsible for an overwhelming majority of the fatigue crack growth damage.
- The predicted fatigue crack growth for the $K14_{10x}$ spectrum indicated a 20% difference between the a_{4x} and a_c values. Although a larger percentage of the load steps in this spectrum were generating fatigue crack damage, the dominant stress ranges were small, and the resulting stress-intensity factor ranges would be less than 1 ksi inch$^{1/2}$.

Conclusions

The results from this analysis indicate that the provided LC-2 pad stay and rollout spectrum components would not produce significant fatigue crack growth on the CM-to-SM flange-to-skin weld. The conservative assumptions used in the analysis give confidence that the results would provide a lower bound for all uncertainties other than increased spectrum severity or structural configuration changes. Thus, from a fatigue crack growth standpoint, no stabilization is required to reduce the LC-2 pad stay and rollout cyclic stresses on the CM-to-SM flange-to-skin weld. This analysis does not represent a complete critical initial flaw size (CIFS) study for the CM-to-SM flange-to-skin weld, or any other component of the structure. The analysis does indicate that the provided LC-2 pad stay and rollout spectrum components will not adversely influence the CIFS if a complete CIFS study were to be performed.

References

(1) Cheston, D., "Independent Evaluation of the Critical Initial Flaw Size for Ares I-X (AIX) Upper Stage Simulator (USS) Common Segment Flange-to-Skin Welds," NASA Engineering and Safety Center Technical Report RP-08-09, February 26, 2008.

(2) Rice, J.R., "A Path Independent Integral and the Approximate Analysis of Strain Concentrations by Notches and Cracks," J. Applied Mechanics, Trans. ASME, Vol. 35, pp. 379-386, 1968.

(3) Goldish, Judy, Boeing Huntington Beach, information provided by email, April 2008.

(4) Pappa, Richard, NASA Langley Research Center, information provided by email, April 2008.

(5) ASTM E 1647, "Standard Test Method for Measurement of Fracture Toughness," Annual Book of ASTM Standards, Volume 3.01, American Society for Testing and Materials, West Conshohocken, Pennsylvania, 2000.

(6) "NASGRO Fracture Mechanics and Fatigue Crack Growth Analysis Software," v5.2, Southwest Research Institute, January 2008.

(7) ASTM E 1820, "Standard Test Method for Measurement of Fracture Toughness," Annual Book of ASTM Standards, Volume 3.01, American Society for Testing and Materials, West Conshohocken, Pennsylvania, 2000.

Appendix A: LC-2 Spectra

Simplified K14 Spectrum

K14 M001				K14 M002			
Cycles	S_{min} (ksi)	S_{max} (ksi)	ΔS (ksi)	Cycles	S_{min} (ksi)	S_{max} (ksi)	ΔS (ksi)
16066	-0.1	0	0.1	13183314	-0.1	0	0.1
49622	-0.2	0	0.2	92303	-0.2	0	0.2
5476	-0.1	0.1	0.2	9	-0.1	0.1	0.2
842	-0.3	0	0.3	6862	-0.2	0.1	0.3
27304	-0.2	0.1	0.3	1175	-0.3	0.1	0.4
27	-0.1	0.2	0.3	28	-0.2	0.2	0.4
17	-0.4	0	0.4	2	-0.4	0.1	0.5
1561	-0.3	0.1	0.4	741	-0.3	0.2	0.5
609	-0.2	0.2	0.4	2	-0.3	0.3	0.6
144	-0.4	0.1	0.5	158	-0.4	0.2	0.6
134	-0.3	0.2	0.5	164	-0.4	0.3	0.7
3	-0.2	0.3	0.5	10	-0.5	0.3	0.8
64	-0.3	0.3	0.6	2	-0.4	0.4	0.8
33	-0.4	0.2	0.6	3	-0.5	0.4	0.9
30	-0.4	0.3	0.7				
6	-0.3	0.4	0.7				
46	-0.5	0.2	0.7				
4	-0.5	0.3	0.8				
37	-0.6	0.3	0.9				
K14 M003				K14 M004			
Cycles	S_{min} (ksi)	S_{max} (ksi)	ΔS (ksi)	Cycles	S_{min} (ksi)	S_{max} (ksi)	ΔS (ksi)
12025	-0.1	0	0.1	15321	-0.1	0	0.1
51911	-0.2	0	0.2	48960	-0.2	0	0.2
5037	-0.1	0.1	0.2	5093	-0.1	0.1	0.2
901	-0.3	0	0.3	1021	-0.3	0	0.3
27573	-0.2	0.1	0.3	25836	-0.2	0.1	0.3
17	-0.1	0.2	0.3	42	-0.1	0.2	0.3
2205	-0.3	0.1	0.4	1528	-0.3	0.1	0.4
465	-0.2	0.2	0.4	385	-0.2	0.2	0.4
59	-0.3	0.2	0.5	16	-0.4	0.1	0.5
3	-0.2	0.3	0.5	626	-0.3	0.2	0.5
38	-0.5	0.1	0.6	54	-0.2	0.3	0.5
294	-0.4	0.2	0.6	76	-0.3	0.3	0.6
127	-0.4	0.3	0.7	182	-0.4	0.2	0.6
				26	-0.5	0.2	0.7
				2	-0.5	0.4	0.9

K14 M005				K14 M006			
Cycles	S_{min} (ksi)	S_{max} (ksi)	ΔS (ksi)	Cycles	S_{min} (ksi)	S_{max} (ksi)	ΔS (ksi)
8789736	-0.1	0	0.1	11968	-0.1	0	0.1
61393	-0.2	0	0.2	41379	-0.2	0	0.2
2380	-0.2	0.1	0.3	5674	-0.1	0.1	0.2
116	-0.3	0.1	0.4	1401	-0.3	0	0.3
57	-0.3	0.2	0.5	24791	-0.2	0.1	0.3
				106	-0.1	0.2	0.3
				2074	-0.3	0.1	0.4
				562	-0.2	0.2	0.4
				42	-0.3	0.2	0.5
				44	-0.2	0.3	0.5
				1	-0.5	0.4	0.9

K14 M007				K14 M008			
Cycles	S_{min} (ksi)	S_{max} (ksi)	ΔS (ksi)	Cycles	S_{min} (ksi)	S_{max} (ksi)	ΔS (ksi)
12060	-0.1	0	0.1	4396734	-0.1	0	0.1
51566	-0.2	0	0.2	31983	-0.2	0	0.2
6561	-0.1	0.1	0.2	1570	-0.2	0.1	0.3
1189	-0.3	0	0.3	116	-0.3	0.1	0.4
26970	-0.2	0.1	0.3	57	-0.3	0.2	0.5
1	-0.1	0.2	0.3				
48	-0.4	0	0.4				
2298	-0.3	0.1	0.4				
440	-0.2	0.2	0.4				
61	-0.3	0.2	0.5				
2	-0.2	0.3	0.5				
38	-0.5	0.1	0.6				
98	-0.4	0.2	0.6				
127	-0.4	0.3	0.7				

Simplified K54 Spectrum

K54 M001				K54 M002			
Cycles	S_{min} (ksi)	S_{max} (ksi)	ΔS (ksi)	Cycles	S_{min} (ksi)	S_{max} (ksi)	ΔS (ksi)
85	-0.1	0	0.1	76151	-0.1	0	0.1
1535	-0.2	0	0.2	17662	-0.2	0	0.2
463	-0.1	0.1	0.2	220	-0.1	0.1	0.2
623	-0.3	0	0.3	151	-0.3	0	0.3
31161	-0.2	0.1	0.3	913	-0.2	0.1	0.3
10	-0.1	0.2	0.3	28	-0.1	0.2	0.3
5	-0.4	0	0.4	1	-0.4	0	0.4
13340	-0.3	0.1	0.4	82	-0.3	0.1	0.4
206	-0.2	0.2	0.4	88	-0.2	0.2	0.4
22	-0.4	0.1	0.5	1	-0.5	0	0.5
505	-0.3	0.2	0.5	19	-0.4	0.1	0.5
9	-0.2	0.3	0.5	199	-0.3	0.2	0.5
233	-0.4	0.2	0.6	17	-0.2	0.3	0.5
10	-0.4	0.3	0.7	20	-0.3	0.3	0.6
58	-0.5	0.3	0.8	3	-0.5	0.1	0.6
46	-0.6	0.4	1	3	-0.4	0.2	0.6
				5	-0.4	0.3	0.7
				4	-0.6	0.1	0.7

K54 M003				K54 M004			
Cycles	S_{min} (ksi)	S_{max} (ksi)	ΔS (ksi)	Cycles	S_{min} (ksi)	S_{max} (ksi)	ΔS (ksi)
110	-0.1	0	0.1	185	-0.1	0	0.1
1779	-0.2	0	0.2	2417	-0.2	0	0.2
461	-0.1	0.1	0.2	516	-0.1	0.1	0.2
681	-0.3	0	0.3	810	-0.3	0	0.3
35211	-0.2	0.1	0.3	33179	-0.2	0.1	0.3
13	-0.1	0.2	0.3	8	-0.1	0.2	0.3
5	-0.4	0	0.4	2	-0.4	0	0.4
15185	-0.3	0.1	0.4	10738	-0.3	0.1	0.4
262	-0.2	0.2	0.4	288	-0.2	0.2	0.4
41	-0.4	0.1	0.5	18	-0.4	0.1	0.5
539	-0.3	0.2	0.5	461	-0.3	0.2	0.5
3	-0.2	0.3	0.5	2	-0.3	0.3	0.6
291	-0.4	0.2	0.6	126	-0.4	0.2	0.6
19	-0.4	0.3	0.7	45	-0.4	0.3	0.7
58	-0.5	0.3	0.8	12	-0.5	0.4	0.9
46	-0.6	0.4	1	24	-0.6	0.4	1

K54 M005			
Cycles	S_{min} (ksi)	S_{max} (ksi)	ΔS (ksi)
209178	-0.1	0	0.1
118753	-0.2	0	0.2
718	-0.1	0.1	0.2
9	-0.3	0	0.3
1149	-0.2	0.1	0.3
38	-0.3	0.1	0.4
5	-0.2	0.2	0.4
6	-0.3	0.2	0.5

K54 M006			
Cycles	S_{min} (ksi)	S_{max} (ksi)	ΔS (ksi)
11968	-0.1	0	0.1
41379	-0.2	0	0.2
5674	-0.1	0.1	0.2
1401	-0.3	0	0.3
24791	-0.2	0.1	0.3
106	-0.1	0.2	0.3
2074	-0.4	0	0.4
562	-0.3	0.1	0.4
42	-0.2	0.2	0.4
44	-0.4	0.1	0.5
1	-0.3	0.2	0.5

K54 M007			
Cycles	S_{min} (ksi)	S_{max} (ksi)	ΔS (ksi)
142	-0.1	0	0.1
2501	-0.2	0	0.2
470	-0.1	0.1	0.2
902	-0.3	0	0.3
31955	-0.2	0.1	0.3
5	-0.1	0.2	0.3
4	-0.4	0	0.4
11856	-0.3	0.1	0.4
285	-0.2	0.2	0.4
23	-0.4	0.1	0.5
466	-0.3	0.2	0.5
1	-0.2	0.3	0.5
67	-0.4	0.2	0.6
18	-0.4	0.3	0.7
6	-0.5	0.3	0.8
12	-0.6	0.4	1

K54 M008			
Cycles	S_{min} (ksi)	S_{max} (ksi)	ΔS (ksi)
104689	-0.1	0	0.1
59705	-0.2	0	0.2
379	-0.1	0.1	0.2
9	-0.3	0	0.3
708	-0.2	0.1	0.3
38	-0.3	0.1	0.4
5	-0.2	0.2	0.4
6	-0.3	0.2	0.5

Simplified K64 Spectrum

K64 M001				K64 M002			
Cycles	S_{min} (ksi)	S_{max} (ksi)	ΔS (ksi)	Cycles	S_{min} (ksi)	S_{max} (ksi)	ΔS (ksi)
93	-0.1	0	0.1	85746	-0.1	0	0.1
3747	-0.2	0	0.2	12948	-0.2	0	0.2
85	-0.1	0.1	0.2	263	-0.1	0.1	0.2
177	-0.3	0	0.3	211	-0.3	0	0.3
41991	-0.2	0.1	0.3	4427	-0.2	0.1	0.3
4133	-0.3	0.1	0.4	41	-0.1	0.2	0.3
579	-0.2	0.2	0.4	12	-0.4	0	0.4
101	-0.4	0.1	0.5	277	-0.3	0.1	0.4
546	-0.3	0.2	0.5	1	-0.1	0.3	0.4
15	-0.4	0.2	0.6	250	-0.2	0.2	0.4
4	-0.4	0.3	0.7	36	-0.4	0.1	0.5
7	-0.5	0.4	0.9	107	-0.3	0.2	0.5
				1	-0.2	0.3	0.5
				2	-0.3	0.3	0.6
				55	-0.4	0.2	0.6
				1	-0.4	0.3	0.7
				5	-0.3	0.4	0.7

K64 M003				K64 M004			
Cycles	S_{min} (ksi)	S_{max} (ksi)	ΔS (ksi)	Cycles	S_{min} (ksi)	S_{max} (ksi)	ΔS (ksi)
621	-0.1	0	0.1	499	-0.1	0	0.1
15108	-0.2	0	0.2	13575	-0.2	0	0.2
312	-0.1	0.1	0.2	350	-0.1	0.1	0.2
489	-0.3	0	0.3	295	-0.3	0	0.3
44202	-0.2	0.1	0.3	38750	-0.2	0.1	0.3
3	-0.1	0.2	0.3	4	-0.1	0.2	0.3
1	-0.4	0	0.4	2034	-0.3	0.1	0.4
2406	-0.3	0.1	0.4	354	-0.2	0.2	0.4
403	-0.2	0.2	0.4	76	-0.4	0.1	0.5
88	-0.4	0.1	0.5	404	-0.3	0.2	0.5
687	-0.3	0.2	0.5	11	-0.2	0.3	0.5
18	-0.2	0.3	0.5	42	-0.3	0.3	0.6
23	-0.3	0.3	0.6	4	-0.5	0.1	0.6
9	-0.4	0.2	0.6	6	-0.4	0.2	0.6
102	-0.4	0.3	0.7	4	-0.4	0.3	0.7
1	-0.5	0.2	0.7	2	-0.5	0.2	0.7
				10	-0.4	0.4	0.8

K64 M007				K64 M008			
Cycles	S_{min} (ksi)	S_{max} (ksi)	ΔS (ksi)	Cycles	S_{min} (ksi)	S_{max} (ksi)	ΔS (ksi)
573	-0.1	0	0.1	37375	-0.1	0	0.1
14236	-0.2	0	0.2	14914	-0.2	0	0.2
331	-0.1	0.1	0.2	111	-0.1	0.1	0.2
419	-0.3	0	0.3	15	-0.3	0	0.3
45605	-0.2	0.1	0.3	3576	-0.2	0.1	0.3
5	-0.1	0.2	0.3	19	-0.1	0.2	0.3
1	-0.4	0	0.4	53	-0.3	0.1	0.4
2318	-0.3	0.1	0.4	45	-0.2	0.2	0.4
1	-0.1	0.3	0.4	20	-0.3	0.2	0.5
553	-0.2	0.2	0.4				
91	-0.4	0.1	0.5				
641	-0.3	0.2	0.5				
17	-0.2	0.3	0.5				
25	-0.3	0.3	0.6				
8	-0.4	0.2	0.6				
100	-0.4	0.3	0.7				
1	-0.5	0.2	0.7				

Appendix B: Sample NASGRO Input File

```
FLAGUI                                  [NASGRO(R) v5.11 final]

[section: general]
[elasticplastic]                        0
[units]                                 0
[calcmode]                              0
[end section]

[section: geometry]
[crackmodel]                            sc17
[geobox0]                               .5
[geobox1]                               678
[geobox2]                               339
[geobox3]                               .1
[geobox4]                               .02
[stressqcount]                          1
[wftype1]                               0
[userornde]                             0
[end section]

[section: material]
[materialcount]                         1
[retardationtype]                       0
[datasource]                            2
[dataformat]                            0
[matcategory]                           F
[matgroup]                              5
[matparam]                              150 150     62      .       .       .
                                        .   0.0015  0.2
[eqnparam]                              6e-10       2.8     0       0       0.001
                                        .01 0.1     .       5.845   1
[cth]                                   1
[useralloycode]
[useralloydesc]
[userheatcode]
[userheatdesc]
[kcoption]                              0
[kcvalue]                               62
[suppressclosure]                       0
[matenvdadn]                            0
[matenvdadnvalue]                       1
[end section]

[section: schedule]
[blockcount]                            8
[flighthourcheck]                       0
[startblock0]
[blocktype]                             1
[blockmanualgridstart]
0                                       .   17      56.6    57      0       0
                                        .   .       .       .
```

1	.	842	56.7	57	0	0
	.	.	.	.		
2	.	49622	56.8	57	0	0
	.	.	.	.		
3	.	16066	56.9	57	0	0
	.	.	.	.		
4	.	144	56.6	57.1	0	0
	.	.	.	.		
5	.	1561	56.7	57.1	0	0
	.	.	.	.		
6	.	27304	56.8	57.1	0	0
	.	.	.	.		
7	.	5476	56.9	57.1	0	0
	.	.	.	.		
8	.	46	56.5	57.2	0	0
	.	.	.	.		
9	.	33	56.6	57.2	0	0
	.	.	.	.		
10	.	134	56.7	57.2	0	0
	.	.	.	.		
11	.	609	56.8	57.2	0	0
	.	.	.	.		
12	.	27	56.9	57.2	0	0
	.	.	.	.		
13	.	37	56.4	57.3	0	0
	.	.	.	.		
14	.	4	56.5	57.3	0	0
	.	.	.	.		
15	.	30	56.6	57.3	0	0
	.	.	.	.		
16	.	64	56.7	57.3	0	0
	.	.	.	.		
17	.	3	56.8	57.3	0	0
	.	.	.	.		
18	.	6	56.7	57.4	0	0
	.	.	.	.		
end						
[blockmanualgridend]						
[blockkeacrow]						
[scalefactor]	1	0	1	0		
[limitstresscheck]	0					
[keaccheck]	0					
[flighthourvalue]	1.0					
[endblock0]						
[startblock1]						
[blocktype]	1					
[blockmanualgridstart]						
0	.	92303	56.8	57	0	0
	.	.	.	.		
1	.	13183314		56.9	57	0
	0	.	.	.	.	
2	.	2	56.6	57.1	0	0
	.	.	.	.		
3	.	1175	56.7	57.1	0	0
	.	.	.	.		

4	.	6862	56.8	57.1	0	0
	.	.	.	.		
5	.	9	56.9	57.1	0	0
	.	.	.	.		
6	.	158	56.6	57.2	0	0
	.	.	.	.		
7	.	741	56.7	57.2	0	0
	.	.	.	.		
8	.	28	56.8	57.2	0	0
	.	.	.	.		
9	.	10	56.5	57.3	0	0
	.	.	.	.		
10	.	164	56.6	57.3	0	0
	.	.	.	.		
11	.	2	56.7	57.3	0	0
	.	.	.	.		
12	.	3	56.5	57.4	0	0
	.	.	.	.		
13	.	2	56.6	57.4	0	0
	.	.	.	.		

end
[blockmanualgridend]
[blockkeacrow]
[scalefactor] 1 0 1 0
[limitstresscheck] 0
[keaccheck] 0
[flighthourvalue] 1.0
[endblock1]
[startblock2]
[blocktype] 1
[blockmanualgridstart]

0	.	901	56.7	57	0	0
	.	.	.	.		
1	.	51911	56.8	57	0	0
	.	.	.	.		
2	.	12025	56.9	57	0	0
	.	.	.	.		
3	.	38	56.5	57.1	0	0
	.	.	.	.		
4	.	2205	56.7	57.1	0	0
	.	.	.	.		
5	.	27573	56.8	57.1	0	0
	.	.	.	.		
6	.	5037	56.9	57.1	0	0
	.	.	.	.		
7	.	294	56.6	57.2	0	0
	.	.	.	.		
8	.	59	56.7	57.2	0	0
	.	.	.	.		
9	.	465	56.8	57.2	0	0
	.	.	.	.		
10	.	17	56.9	57.2	0	0
	.	.	.	.		
11	.	127	56.6	57.3	0	0
	.	.	.	.		

12	.	3	56.8	57.3	0	0
	.	.	.	.		
end						
[blockmanualgridend]						
[blockkeacrow]						
[scalefactor]	1	0	1	0		
[limitstresscheck]	0					
[keaccheck]	0					
[flighthourvalue]	1.0					
[endblock2]						
[startblock3]						
[blocktype]	1					
[blockmanualgridstart]						
0	.	1021	56.7	57	0	0
	.	.	.	.		
1	.	48960	56.8	57	0	0
	.	.	.	.		
2	.	15321	56.9	57	0	0
	.	.	.	.		
3	.	16	56.6	57.1	0	0
	.	.	.	.		
4	.	1528	56.7	57.1	0	0
	.	.	.	.		
5	.	25836	56.8	57.1	0	0
	.	.	.	.		
6	.	5093	56.9	57.1	0	0
	.	.	.	.		
7	.	26	56.5	57.2	0	0
	.	.	.	.		
8	.	182	56.6	57.2	0	0
	.	.	.	.		
9	.	626	56.7	57.2	0	0
	.	.	.	.		
10	.	385	56.8	57.2	0	0
	.	.	.	.		
11	.	42	56.9	57.2	0	0
	.	.	.	.		
12	.	76	56.7	57.3	0	0
	.	.	.	.		
13	.	54	56.8	57.3	0	0
	.	.	.	.		
14	.	2	56.5	57.4	0	0
	.	.	.	.		
end						
[blockmanualgridend]						
[blockkeacrow]						
[scalefactor]	1	0	1	0		
[limitstresscheck]	0					
[keaccheck]	0					
[flighthourvalue]	1.0					
[endblock3]						
[startblock4]						
[blocktype]	1					
[blockmanualgridstart]						
0	.	61393	56.8	57	0	0
	.	.	.	.		

1 . 878973 56.9 57 0 0
. . . .
2 . 116 56.7 57.1 0 0
. . . .
3 . 2380 56.8 57.1 0 0
. . . .
4 . 57 56.7 57.2 0 0
. . . .
end
[blockmanualgridend]
[blockkeacrow]
[scalefactor] 1 0 1 0
[limitstresscheck] 0
[keaccheck] 0
[flighthourvalue] 1.0
[endblock4]
[startblock5]
[blocktype] 1
[blockmanualgridstart]
0 . 1401 56.7 57 0 0
. . . .
1 . 41379 56.8 57 0 0
. . . .
2 . 11968 56.9 57 0 0
. . . .
3 . 2074 56.7 57.1 0 0
. . . .
4 . 24791 56.8 57.1 0 0
. . . .
5 . 5674 56.9 57.1 0 0
. . . .
6 . 42 56.7 57.2 0 0
. . . .
7 . 562 56.8 57.2 0 0
. . . .
8 . 106 56.9 57.2 0 0
. . . .
9 . 44 56.8 57.3 0 0
. . . .
10 . 1 56.5 57.4 0 0
. . . .
end
[blockmanualgridend]
[blockkeacrow]
[scalefactor] 1 0 1 0
[limitstresscheck] 0
[keaccheck] 0
[flighthourvalue] 1.0
[endblock5]
[startblock6]
[blocktype] 1
[blockmanualgridstart]
0 . 48 56.6 57 0 0
. . . .
1 . 1189 56.7 57 0 0
. . . .

2	.	51566	56.8	57	0	0
	.	.	.	.		
3	.	12060	56.9	57	0	0
	.	.	.	.		
4	.	38	56.5	57.1	0	0
	.	.	.	.		
5	.	2298	56.7	57.1	0	0
	.	.	.	.		
6	.	26970	56.8	57.1	0	0
	.	.	.	.		
7	.	6561	56.9	57.1	0	0
	.	.	.	.		
8	.	98	56.6	57.2	0	0
	.	.	.	.		
9	.	61	56.7	57.2	0	0
	.	.	.	.		
10	.	440	56.8	57.2	0	0
	.	.	.	.		
11	.	1	56.9	57.2	0	0
	.	.	.	.		
12	.	127	56.6	57.3	0	0
	.	.	.	.		
13	.	2	56.8	57.3	0	0
	.	.	.	.		
end						
[blockmanualgridend]						
[blockkeacrow]						
[scalefactor]	1	0	1	0		
[limitstresscheck]	0					
[keaccheck]	0					
[flighthourvalue]	1.0					
[endblock6]						
[startblock7]						
[blocktype]	1					
[blockmanualgridstart]						
0	.	31983	56.8	57	0	0
	.	.	.	.		
1	.	439673	56.9	57	0	0
	.	.	.	.		
2	.	116	56.7	57.1	0	0
	.	.	.	.		
3	.	1570	56.8	57.1	0	0
	.	.	.	.		
4	.	57	56.7	57.2	0	0
	.	.	.	.		
end						
[blockmanualgridend]						
[blockkeacrow]						
[scalefactor]	1	0	1	0		
[limitstresscheck]	0					
[keaccheck]	0					
[flighthourvalue]	1.0					
[endblock7]						
[netsectionstresscheck]	0					
[schedtitle]	CMLAS					
[schedcount]	2000					

[startschedassembly]

0	1 1
1	2 1
2	3 1
3	4 1
4	5 1
5	6 1
6	7 1
7	8 1

end
[endschedassembly]
[end section]

[section: output]
[sessiontitle]
[damageeditingtitle]Damage Edit

[maxdamageremoved]	0.0
[schedulenumber]	2
[printoption]	0
[schedprintinterval]	1
[blockprintinterval]	1
[stepprintinterval]	1
[stepdetailprintinterval]	0
[cremen]	0.005
[cyclebycyclemode]	0
[plotoption]	0

[end section]

[section: multirun]

[crackmultirun]	0

[end section]

REPORT DOCUMENTATION PAGE

Form Approved
OMB No. 0704-0188

1. REPORT DATE *(DD-MM-YYYY)*	2. REPORT TYPE	3. DATES COVERED *(From - To)*
01- 10 - 2008	Technical Memorandum	

4. TITLE AND SUBTITLE
Assessment of the LC-2 Prelaunch Fatigue Spectra of the CM-to-SM Flange Weld

5a. CONTRACT NUMBER

5b. GRANT NUMBER

5c. PROGRAM ELEMENT NUMBER

6. AUTHOR(S)
Dawicke, David S.; and Newman, John A.

5d. PROJECT NUMBER

5e. TASK NUMBER

5f. WORK UNIT NUMBER
698259.02.07.07.03.02

7. PERFORMING ORGANIZATION NAME(S) AND ADDRESS(ES)
NASA Langley Research Center
Hampton, VA 23681-2199

8. PERFORMING ORGANIZATION REPORT NUMBER
L-19525

9. SPONSORING/MONITORING AGENCY NAME(S) AND ADDRESS(ES)
National Aeronautics and Space Administration
Washington, DC 20546-0001

10. SPONSOR/MONITOR'S ACRONYM(S)
NASA

11. SPONSOR/MONITOR'S REPORT NUMBER(S)
NASA/TM-2008-215529

12. DISTRIBUTION/AVAILABILITY STATEMENT
Unclassified - Unlimited
Subject Category 39
Availability: NASA CASI (301) 621-0390

13. SUPPLEMENTARY NOTES

14. ABSTRACT

A fatigue crack growth analysis was conducted that used loads (LC-2) and stress analyses developed by the Ares I-X Project and utilized material data and analysis methods developed by a critical initial flaw size (CIFS) analysis conducted by NASA Engineering and Safety Center (NESC) for the Upper Stage Simulator (USS) of the Ares I-X vehicle. A full CIFS analysis for the CM-to-SM flange-to-skin weld was not performed because the full flight spectrum was not provided and was not necessary to answer the question posed by the Ares I-X Project. Instead, an approach was developed to determine if the crack growth due to the pad stay and rollout components of the flight spectrum would adversely influence the CIFS. The results from this analysis indicate that the LC-2 pad stay and rollout spectrum components would not produce significant fatigue crack growth on the CM-to-SM flange-to-skin weld.

15. SUBJECT TERMS
Residual Stresses; Fatigue crack; Critical initial flaw size; Damage-tolerance; Ares I-X

16. SECURITY CLASSIFICATION OF:			17. LIMITATION OF ABSTRACT	18. NUMBER OF PAGES	19a. NAME OF RESPONSIBLE PERSON
a. REPORT	b. ABSTRACT	c. THIS PAGE			STI Help Desk (email: help@sti.nasa.gov)
					19b. TELEPHONE NUMBER *(Include area code)*
U	U	U	UU	34	(301) 621-0390